New density profile reconstruction methods for X-mode reflectometry

R. B. Morales[1], S. Hacquin[2,3], S. Heuraux[1], and R. Sabot[2]

[1] *IJL, University of Lorraine, UMR 7198 CNRS, 54506 Vandoeuvre, France*
[2] *IRFM, CEA Cadarache, 13108 Saint-Paul-lez-Durance, France*
[3] *EUROfusion Programme Management Unit, Culham Science Centre, Culham, OX14 3DB, United Kingdom*

1 Motivation

This contribution presents new data analysis techniques to improve the density profile reconstruction for frequency swept X-mode reflectometry. This effort undergoes in three fronts: the initialization of the reconstruction; the inversion method that reconstructs the density profile; and the description of blind areas to the reflectometer. The description of blind areas is the subject of an additional contribution in this same workshop. The initialization technique is assumed well implemented by the established techniques described in Refs. [1, 2] and will be further accessed in the future. The focus of this contribution is on new inversion techniques.

2 New integration shapes and accuracy benchmarking

The method published by Bottollier-Curtet et al [3] has been the standard density profile reconstruction method in X-mode reflectometry ever since. To improve the accuracy of the reconstruction method, shapes more complex than linear for the last integration step of the refractive index were investigated. The shapes tested included parabolas, square root and x^α, with α between zero and 1/2. The exponent α can be demonstrated to be directly translated to an integration weight factor named W, with $W = 1/(\alpha+1)$. The detailed development of each method can be found in reference [4]. The benchmarks were performed on the synthetic profiles shown in Fig. 1. Synthetic data was used because it is the only way to know how precise was the profile reconstruction. It is also the most accurate way to enforce the reconstruction conditions in the initialization and the noise level.

By working with the synthetic profiles shown in Fig. 1, the ideal refractive index shapes of the type x^α can be accessed. The respective W profile is shown in Fig. 2.

Initially, the profile of the ideal W given in Fig. 2 is used to benchmark the reconstruction accuracies and later on, the methods to determine the W factors are discussed. Applying all methods introduced on the synthetic profiles of Fig. 1 yields the reconstruction discrepancy profiles presented in Fig. 3.

Starting with the parabolic implementation, the reconstruction accuracy starts less accurate than the linear method in the plasma edge and becomes slightly more accurate in the plasma core. However in this case no stabilization parameter was necessary. Implementing the square root integration shape yield a more accurate reconstruction overall, but specially in the plasma core. This is because the square root shape describes very accurately the refractive index shape in these conditions. Optimizing the integration weight factor W made the reconstruction more accurate and stable in the plasma edge, achieving stable sub-millimeter precision across the entire profile.

3 Analysis of the reconstruction stability

The linear Bottollier-Curtet's algorithm (when W=1/2) turned out to be unstable and a stabilization mechanism was introduced. The measured phase shift of each frequency step is averaged

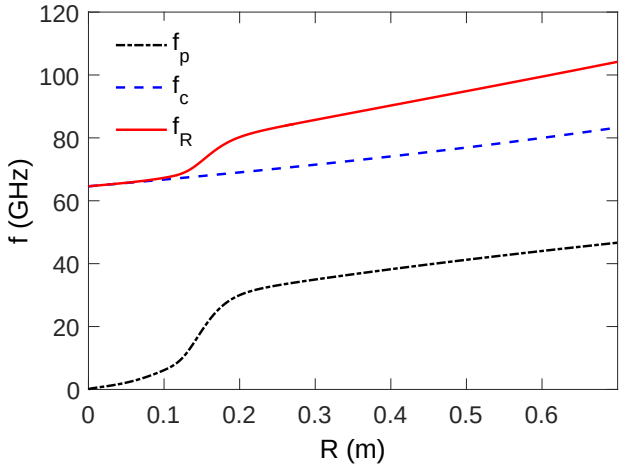

Figure 1: Frequency profiles from typical Tore Supra discharges including a pedestal located at R=12 cm and B=2 T at the plasma center.

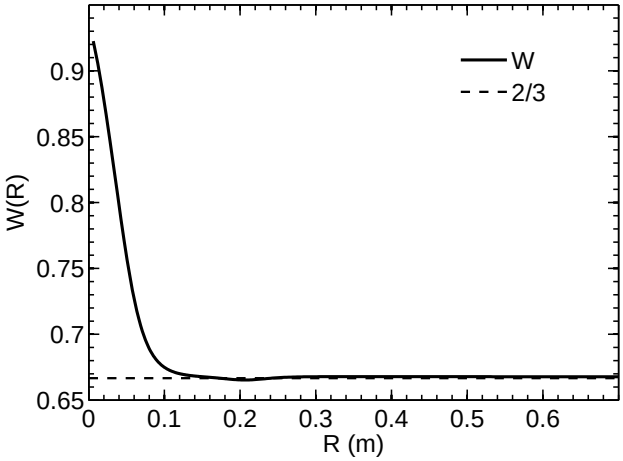

Figure 2: Profile of weight factors W for the typical Tore Supra profiles example as depicted in Fig. 1.

with the value of the previous step. In order to analyse the stabilization mechanisms, the recursive formula for the computation of each radial step can be written in a simplified way as:

$$\Delta R = \frac{\Delta\phi}{WN}, \tag{1}$$

with ΔR being the radial step normalized by the probing wavelength $(R_n - R_{n-1})/\lambda_n$, $\Delta\phi$ being the phase increment of the probing frequency f_n from R_{n-1} to R_n, normalized by 2π, and N being $N(f_n, R_{n-1})$.

First, the averaging with the previous step, as in the linear Bottollier-Curtet solution, was tested for every component of Eq. 1 (the radial step, the phase shift and the value of N_{n-1}). The conclusion is that there is no preferred component to be stabilized. The best component to stabilize varies depending on the profile to be reconstructed. Next, the numerical stability is investigated by the propagation of errors in each element of Eq. 1. An error in the evaluation of $N(R_{n-1})$ and $\Delta\phi^{R_n}_{R_{n-1}}$ comes from an error in the determination of R_{n-1}. Meaning that an error in the position R_n is due to not using the ideal value for W, plus the error propagated from the previous

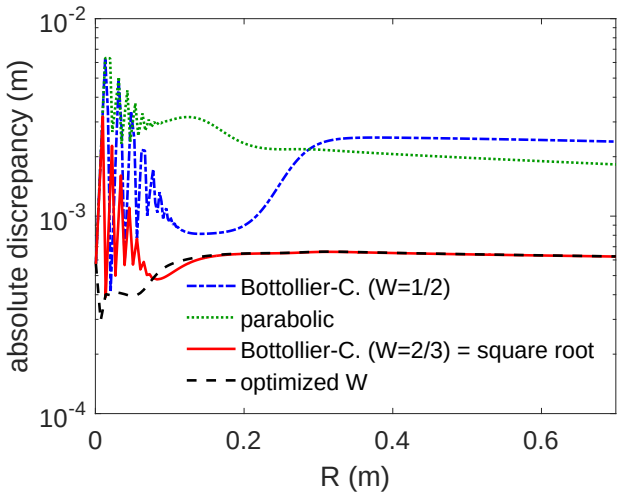

Figure 3: Profiles of absolute radial discrepancy when reconstructing the density profile with the conditions of 500 probing frequencies, a precision of 0.1 mm in the initialization and the Tore Supra example profiles as depicted in Fig. 1.

position into $\Delta\phi$ and N. The propagation of these error sources in ϕ, W and N, can be evaluated by equating them as in Eqs. 2 to 4, respectively. The error in $\Delta\phi$ is additive, whereas in W and N, the error is introduced as a multiplicative factor ϵ and ζ, respectively.

$$\frac{1}{W}\frac{(\Delta\phi+\Delta\phi')}{N} = \frac{1}{W}\frac{\Delta\phi}{N} + \frac{1}{W}\frac{\Delta\phi'}{N} \tag{2}$$

$$\frac{1}{\epsilon W}\frac{\Delta\phi}{N} = \frac{1}{W}\frac{\Delta\phi}{N} + \left(\frac{1-\epsilon}{\epsilon}\right)\frac{1}{W}\frac{\Delta\phi}{N} \tag{3}$$

$$\frac{1}{W}\frac{\Delta\phi}{\zeta N} = \frac{1}{W}\frac{\Delta\phi}{N} + \frac{1}{W}\left(\frac{1-\zeta}{\zeta}\right)\frac{\Delta\phi}{N} \tag{4}$$

All reconstruction steps are subject to the error of not using the ideal local value of W, plus the error propagating from the previous steps. Directly from Eqs. 2 to 4, it can be observed that the errors in the evaluation of the phase shift will be multiplied by the factor $1/WN$, whereas the errors in the refractive index and weight factor are multiplied by $\Delta\phi/WN$. Furthermore, any error in each element of Eq. 1 induces an oscillation. For example, an excess in R_n causes an excess in the computed $\Delta\phi_0^n$ for the frequency f_{n+1}. Which causes an under evaluation of $\Delta\phi_n^{n+1}$, resulting in under evaluating R_{n+1}. These errors are damped or not depending on these error multiplicative factors written in Eqs. 2 to 4.

The combination of these facts shows that the more efficient scenario to damp errors is when WN is greater. Because the error is multiplied by $1/WN$ in the next step. Furthermore, the reconstruction only damps the previous errors when $1/W$ is between one and two (the step function and linear cases). For $1/W$ equals or greater than two there is no damping of errors. These conclusions come from the oscillatory character explained. An error of $+E$ in one step translates into an error of $-E$ in the next step. When this error is multiplied by one, the best damping occurs because $+E - 1 \times E = 0$. When it is multiplied by two, no damping occurs because $+E - 2 \times E = -E$. Since there is no error damping and an additional error is introduced in every step by not using the perfect value of W, the system becomes unstable. This interpretation explains why it is observed that the square root integration shape converges, unlike the linear integration, and when the factor W and N are closer to one that any error introduced is damped more efficiently. This last feature is observed in the edge conditions in the next section. A last remark is that this analysis is done focusing on the true local values of W. Using $W = 1$ when it is not the ideal value can be interpreted as if the damping efficiency is not of $W = 1$, but of the ideal

local value itself, and in addition, an error is introduced from the excess in W, as it was shown in Eq. 3.

4 Noise analysis

In experimental data there are always many sources of noise. This section shows the impact on the reconstruction accuracy from adding white noise and localized spikes in the phase signal. First, a spike of 1% is added in the phase shift of a single frequency. The radial error at the location where the phase shift spike was introduced is presented in Fig. 4.

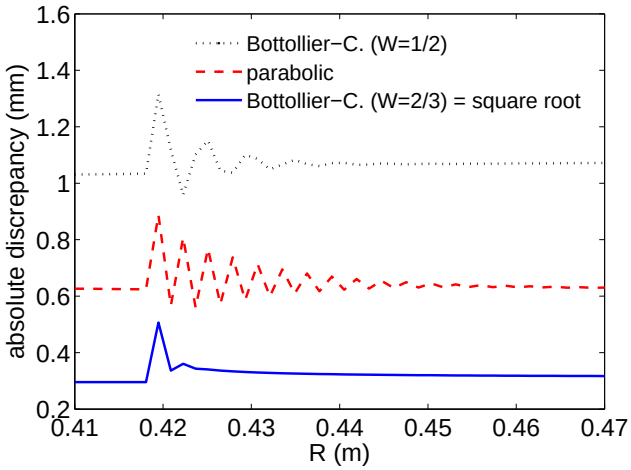

Figure 4: Radial discrepancy when reconstructing the density profile with a 1% spike in the phase shift of a single frequency and conditions of 500 probing frequencies, a precision of 0.1 mm in the initialization and the linear f_R profile.

Fig. 4 shows that an error introduced is damped faster for the square root method. The parabolic method enforced boundary conditions to find the parabolas and this made the error propagate longer. Small density perturbations were also tested but they had the same features as presented in the phase shift case in Fig. 4.

Next, white noise is added to the phase shift data, as a percentage of the average value, to simulate the experimental noise in the Tore Supra example. Fig. 5 shows the obtained accuracies for the reconstruction methods with fixed $W = 2/3$ and optimized W profile, at two different noise levels. From the interpretations on the last section, one can verify how indeed the edge region is very efficient in damping the noise introduced since $1/WN$ is minimized. This is an interesting feature of the reconstruction method since the edge region is typically more prone to noise and fluctuations in tokamaks. In the core region, on the other hand, the discrepancy saturates at a higher value, depending on the noise level. All methods showed the exact same tendency. They retain the same discrepancies in the edge region for all noise levels and linearly increase in the core as the noise level increases. The parabolic method is not represented because it was able to find the parabolas only with a maximum noise level up to 1%. Beyond this level of noise, the method is unable to associate parabolas for the data in too many cases and the method collapses to the linear solution.

5 Methods to find the profile of the integration factor W

The first method to implement an optimized W profile is to do it iteratively. At each profile reconstruction, a simulation can determine the optimized values of W based on the profile previously reconstructed. However, this is the most computational demanding approach to this problem. On the other hand, for a specific well known case, taking the solution in Fig. 2 as example, the ideal

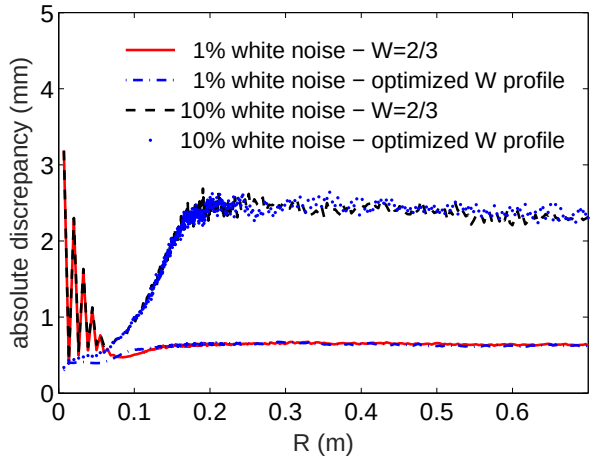

Figure 5: Radial discrepancy when reconstructing the density profile with different levels of white noise in the phase shift data and conditions of 500 probing frequencies, a precision of 0.1 mm in the initialization and the typical low B Tore Supra example profile. Each discrepancy profile is the average of 500 reconstructions.

W profile can be determined beforehand. The transition from $W \sim 1$ to $W = 2/3$ is quite linear in this case and the position where W converges to 2/3 is clearly marked by the presence of a pedestal. In these two implementations, the bottleneck parameters are the assumption of the first value of W and the compatibility of the profile shape. Although these methods were tested and showed improved reconstruction accuracy, the most general, reliable and accurate implementation is to determine the factor W at each frequency step based on the local plasma parameters. This solution is fully developed in Ref. [4]. The obtained expression for W is:

$$W(N_{n-1}, f_R, \nabla f_R) = \frac{1}{\alpha(N_{n-1}, f_R, \nabla f_R) + 1}, \tag{5}$$

$$\alpha(N_{n-1}, f_R, \nabla f_R) = 0.5 - 0.5[\gamma(f_R, \nabla f_R) N_{n-1}^2 + \delta(f_R, \nabla f_R) N_{n-1}^{4.44}], \tag{6}$$

$$\gamma(f_R, \nabla f_R) = p_1(f_R)/[\nabla f_R - p_2(f_R)] + p_3(f_R), \tag{7}$$

$$\delta(f_R, \nabla f_R) = q_1(f_R)/[\nabla f_R - q_2(f_R)] + q_3(f_R), \tag{8}$$

with f_R taken as the probing frequency p_n and q_n given by Eqs. 9 to 14:

$$p_1 = a_1 f_R^2 + b_1 f_R + c_1, \tag{9}$$

$$p_2 = a_2 f_R^6 + b_2 f_R^5 + c_2 f_R^4 + d_2 f_R^3 + e_2 f_R^2 + f_2 f_R + g_2, \tag{10}$$

$$p_3 = a_3 f_R^4 + b_3 f_R^3 + c_3 f_R^2 + d_3 f_R + e_3, \tag{11}$$

$$q_1 = a_1' f_R^3 + b_1' f_R^2 + c_1' f_R + d_1', \tag{12}$$

$$q_2 = a_2' f_R^2 + b_2' f_R + c_2', \tag{13}$$

$$q_3 = a_3' f_R^5 + b_3' f_R^4 + c_3' f_R^3 + d_3' f_R^2 + e_3' f_R + f_3', \tag{14}$$

with all the fitting parameters a_i to g_i and a_i' to f_i' listed in Ref. [4].

This final expression allows to optimize the weight factors W at all frequency steps and achieve the accuracy shown in Fig. 3 for any profile shape that satisfies the boundary conditions assumed when solving for W. An additional application of this solution is to use less probing frequencies for real-time monitoring of fast profile evolution.

6 Reconstructions with less probing frequencies

Up to now, all profile reconstructions obeyed the rule of more probing frequencies results in better accuracy. Which is mainly because the refractive index shape is better described by a square root function the smaller is the radial step. In addition, the error introduced by miscalculating the area under the refractive index curve is proportionally bigger to the increase of the radial step, emphasizing the previous feature. With the results of the previous section, however, the mismatch in the shape of the refractive index can be corrected. Therefore, the profile can be reconstructed using less probing frequencies without loss of accuracy.

Using less probing frequencies speeds up the reconstruction algorithm, allowing for monitoring of faster density profile evolution. This was tested for the Tore Supra example profile when reducing the number of frequencies from 500 to 100 and speeding the reconstruction in roughly five times, depending on the computer set-up. In this case, the fluctuations in the edge region peak at one centimeter when the factor W is fixed at $2/3$. When W is optimized for all steps, the discrepancy profile go back to values below one millimeter.

Other examples that can benefit from optimizing the factor W include cases with very low or high magnetic fields, because the refractive index in the previous cut-off is higher the farther the two frequency profiles, f_{ce} and f_{pe}, are from one another. To demonstrate one case, a low density profile linear in f_R with $\nabla f_R = 20\,GHz/m$ is assumed. In this condition, no pedestal is present and it is not clear where the square root function describes well the refractive index shape. In addition, the number of probing frequencies is reduced to 50. Applying the method developed in the previous section gives the optimized W for each probing frequency as presented in Fig. 6. In this case, the W profile is never too close to the square root method solution of $2/3$, it is always above 0.7. The accuracy of the reconstructed profiles before and after optimizing the W profile are depicted in Fig. 7. A maximum error of 0.4 mm is observed in the reconstructed profile when the W profile is optimized. If reducing even more the number of probing frequencies, the radial steps become too large. In such cases, the error in the trapezoidal integration before the last step surpasses the error from integrating the last radial step. For all cases explored here, the error in the trapezoidal integration surpasses the error in the last step when the radial step surpasses 5 cm.

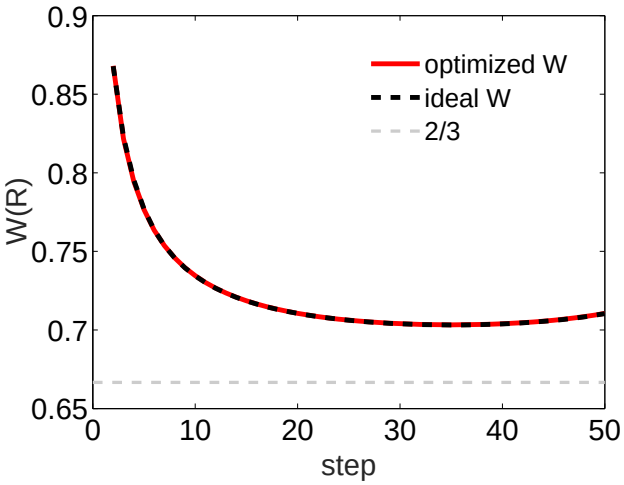

Figure 6: Ideal $W(R)$ and the obtained $W(R)$ from the method of Sec. 5 for a linear f_R profile with $\nabla f_R = 20\,GHz/m$ and only 50 probing frequencies.

The reduction on the number of frequency steps was also tested in the Tore Supra example with the introduction of white noise in the time of flight and phase shift data. When a low level of white noise is introduced, up to 1%, no difference is observed between the cases with 500 or 100 frequencies. For higher levels of noise the discrepancy in the core raises, doubling the noiseless value at around 10% noise level.

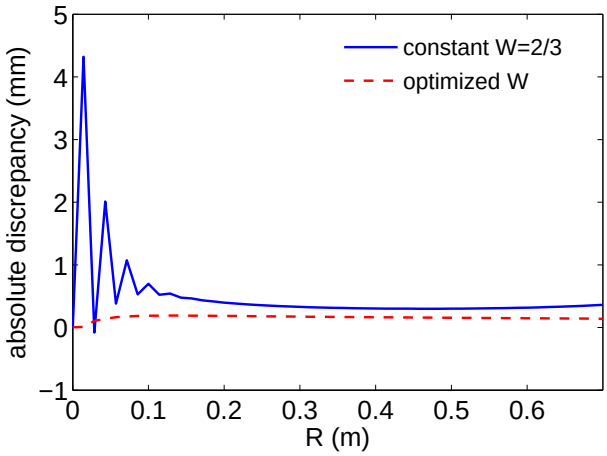

Figure 7: Example of the optimization of the weight factor $W(R)$, as defined in Eq. 5, for a linear f_R profile and only 50 probing frequencies.

7 Conclusions

Following the recent advances and demands in the reflectometry techniques, deeper understanding and additional improvements on the density profile reconstruction method was aimed here in the data analysis front. A crucial point in the reconstruction method is the assumed refractive index shape in the integration over each radial step. The obtained results from all reconstruction methods demonstrated that using appropriate fractional power functions, implemented with the factors $W(R)$, improves the reconstructed profile accuracy and stability because they are a much better match to the true refractive index profiles. Although the use of a square root profile achieved good results in the core plasma, it is not the best suited shape in the edge plasma. In this region, the power of the fractional power functions used to describe the refractive index profile can be very close to zero in the first reflected frequencies. The adaptation of the power of these functions according to the plasma profile showed an accuracy improvement in plasma edge conditions from millimeters to sub-millimeters for the conditions assumed.

The numerical stability analysis showed how the reconstruction is more stable when not using any information of the previously calculated positions to determine the next position, or even, forcing smoother variation on any of the reconstruction terms. All these procedures were demonstrated to delay the error damping capability of the reconstruction method when spurious events and phase noise were introduced. The relations between the noise level, the optimal $W(R)$ and the obtained accuracy were well covered by Fig. 5. The typical edge conditions lead to higher values of WN_{n-1}. It was demonstrated mathematically and observed in Fig. 5 that the higher is WN_{n-1}, the better the reconstruction damps errors and noise. This is a convenient feature for the profile reconstruction since there are typically higher noise levels in the edge plasma. In the core region, on the other hand, the reconstruction error consistently increases as the noise level increases.

When reconstructing a well known density profile shape containing a clear pedestal transition, the optimized integration shapes could be easily proposed. The limitations being the pedestal to be evident and the determination of the first integration shape. The method elaborated in Sec. 5 suppresses these issues. It can be used to determine the entire profile of integration factors for any profile shape. Optimizing the integration factors also allow to use a reduced number of probing frequencies to reconstruct the profile without any accuracy loss, as demonstrated in two examples. This feature enables the real-time monitoring of faster density profile evolution.

References

[1] F. Clairet, C. Bottereau, J. M. Chareau and R. Sabot. Rev. of Sci. Instrum. **74**, 1481 (2003)

[2] F. Clairet, B. Ricaud, F. Briolle, S. Heuraux and C. Bottereau, Rev. of Sci. Instrum. **82**, 083502 (2011)

[3] H. Bottollier-Curtet and G. Ichtchenko, Rev. of Sci. Instrum. **4**, 58 (1987)

[4] R. B. Morales, S. Hacquin, S. Heuraux and R. Sabot, Rev. of Sci. Instrum. **88**, 043503 (2017)